Palacký University Olomouc
Faculty of Science

Department of Optics

Polarization state generation, measurement and control using liquid-crystal modulators

Master's Thesis

Martin Bielak

2019

Palacký University Olomouc
Faculty of Science

Department of Optics

Polarization state generation, measurement and control using liquid-crystal modulators

Master's Thesis

Author:	Bc. et Bc. Martin Bielak
Study programme:	B1701 Physics
Field of study:	Optics and Optoelectronics
Form of study:	Full-time
Supervisor:	RNDr. Miroslav Ježek, Ph.D.

Thesis submitted on: .....

Univerzita Palackého
Přírodovědecká fakulta

Katedra optiky

Příprava, měření a manipulace polarizace světla pomocí kapalných krystalů

Diplomová práce

Autor: Bc. et Bc. Martin Bielak
Studijní program: B1701 Fyzika
Studijní obor: Optika a optoelektronika
Forma studia: Prezenční
Vedoucí: RNDr. Miroslav Ježek, Ph.D.

Práce odevzdána dne: .....

Abstract

The polarization degree of freedom of light is frequently used in optical communication and metrology as well as in quantum information processing. Rotating polarization retarders, such as half wave plate and quarter wave plate, are commonly used in many experiments for polarization analysis. The liquid crystals represent one of the technologies which do not require major interventions in already assembled experimental setups and can enhance the measurements. Particularly, devices made of liquid crystals can be used to speed up polarization preparation and analysis.

This thesis deals with the characterization of device made from liquid crystals cells and its application in polarization preparation and analysis. We discuss an extraction of the liquid crystal cell from a liquid crystal display and the process of its calibration to a reference polarimeter. Also, the theoretical description by means of analytical model and machine learning model is discussed. We present basic imperfections and problems that can be observed in the real-world use of liquid crystal cells and that are not commonly covered by the theoretical models. These phenomena can be included in the machine learning model as it learns and extrapolates from actual measured data. It outperforms significantly the analytical model, which is verified on a large measured data set.

Furthermore, we report on the use of the developed device for various types of polarization tomographic schemes, such as minimum tomography (for states), eigenstates of Pauli operators (three bases or six states), and covariant measurement. We perform a calibration and the tomographic procedure for the first two schemes mentioned. Also, we carried out numerical simulations of an overcomplete tomographic scheme, which converges to the covariant measurement.

The overcomplete measurements are used to demonstrate the reduction of uncertainty in the case of a large number of projections used for analysis and benefits of liquid crystals for this type of measurement. The results which are presented in this thesis show the possibility of using the device made from commercially available liquid crystal displays in polarization preparation, analysis, and polarization encoding of information in general.

Keywords

`polarization, liquid crystal, liquid crystal models, liquid crystal device, segment liquid crystal display, minimal analysis, polarization analysis, polarization preparation, tomographic measurement methods, genetic algorithm, machine learning`

Abstract

Elektrooptická modulace světla pomocí prvků s kapalnými krystaly je využita pro přípravu a měření libovolného polarizačního stavu světla a také pro transformaci mezi různými stavy polarizace klasických i jednofotonových optických signálů. Součástí práce je návrh a realizace vhodných kombinací modulátorů pro dosažení požadovaných polarizačních operací, jejich kalibrace a demonstrace využití ve vybraných experimentech.

Klíčová slova

polarizace, tekuté krystaly, modely tekutch krystalů, zařízení s tekutými krystaly, displej z tekutých krystalů, minimální analýza, analýza polarizace, příprava polarizace, metody tomografického měření, genetický algoritmus, strojové učení

Acknowledgments

First of all, I would like to express my sincere gratitude to my supervisor RNDr. Miroslav Ježek, Ph.D. for guidance, patience, and advice. My thanks also go to my colleagues for a friendly environment, kindes, and mutual help. Last but not least I would like to thank my family for their care and continuous support.

Martin Bielak

Declaration

I hereby declare that I have written this Master's Thesis—and performed all the presented research and experimental tasks—by myself, while being supervised by RNDr. Miroslav Ježek, Ph.D. I also state that every resource used is properly cited. I agree with the Thesis being used for teaching purposes and being made available at the website of the Department of Optics.

Signed in Olomouc on ....

Martin Bielak

Contents

Chapter 1

Introduction

Information about the polarization of the light is important in a vast number of applications. Many works show the benefits of the use of liquid crystals in polarimetry [1–6] and spectrometry [7] compared to mechanical polarimeters. Liquid crystals can be used for the construction of polarization controllers to prepare any state of polarization of light and to change an arbitrary state to another [8]. The device that combines quarter wave plates and liquid crystal can be used as a phase modulator [9, 10]. A pixelized liquid crystal device can be used as a spatial modulator [11–13].

Liquid crystals allow any spatial layout of the active area and they are able to perform different polarization changes on the closely separated optical beams. Also, the rate of the changes of the polarization output is much higher for liquid crystals than for mechanically manipulated wave plates. Together with polarizers, liquid crystals can be used as amplitude modulators and switches [14, 15], or it is possible to use them to create interference filters [16]. Alternatively, electro-optic effect in Pockels cells can be used to change the state of polarization. Pockels cells have some advantages as a rate of transition between individual states is faster than for liquid crystals, but they need a high driving voltage (kV) or they must be waveguide integrated, which brings additional problems.

It is necessary to have a precise theoretical model of liquid crystal operation. The liquid crystal polarization transformation can be described by means of an analytical model expressed in the Jones formalism. In the thesis, I show some examples of models and their advantages and disadvantages. The real-world liquid crystal behavior is different from the one predicted by the models. In the thesis, I deal with some shortcomings of the theoretical models and I show advantages of machine learning for the description of liquid crystal behavior.

Furthermore, I focus on the application of liquid crystals in polarimetry. There are various types of polarization tomographic schemes. The minimal tomogra-

phy [17] utilizes the minimum number of individual projective measurements needed for a complete reconstruction of the polarization state. For example, a classical single-mode polarimeter and a single polarization qubit tomography each require four projections. These individual measurements can be performed sequentially or in the same time by a complex multi-channel detection setup [18], which speeds up data acquisition but requires more optical components and detectors. Another frequently used tomographic scheme consists in projecting the unknown state to eigenstates of Pauli operators, or their direct products in the case of higher dimensional systems. For classical polarimetry or single qubit (two-level systems), these eigenstates are horizontal (H), vertical (V), diagonal (D), anti-diagonal (A), right-handed circular (R), and left-handed circular (L) polarization. Alternatively, projecting to states of mutual-unbiased bases [19] represents another option, though virtually impossible to realize for high-dimensional or multi-partite systems. The mutually-unbiased bases scheme coincides with the Pauli operators eigenstates scheme for two-level systems. This six-projection measurement scheme is over-determined as it provides more detection outputs than the number of independent parameters of the state. In the thesis, I experimentally evaluate the performance of a liquid crystal device consisting of three liquid crystal cells in four-projection as well as six-projection tomographic schemes.

Recently it was reported that increasing the number of projective measurement applied on a polarization state under characterization, while keeping the overall number of photons detected during the whole tomography constant, yields lower uncertainty of the result [20–22]. In the thesis, I perform numerical simulations for 4-projection and 6-projection schemes, and also for 60-projection measurement, which approaches a limit of covariant measurement [20]. The corresponding detection outputs are simulated for randomly generated polarization states, maximum-likelihood estimation is performed, and a distance between the true state and the estimated one is computed and averaged over hundreds of states. I can replicate the uncertainty reduction for increasing number of projection for the ideal detection schemes as well as for imperfect projective measurements performed by the developed liquid crystal device. The experimental verification might be challenging due to high number of states prepared and projections detected. Employing fast projection switching using liquid crystal devices, however, I estimate several hours to several dozens of hours long measurement, which will be subject of future work.

Even though the minimal tomography requires fewer voltage changes and usually takes less time, sometimes it is not appropriate to reduce the number of projections. To demonstrate the benefits of a large number of projectors, I have

used the ability of a constructed liquid crystal device to switch quickly between any polarization projection. To combine the benefits of minimal tomography, H, V, D, A, R, L analyzes and many projection analysis, we decided to develop a device configuration that allows switching between these modes of tomography only by changing combinations of the applied voltages on twisted nematic liquid crystal cells.

Chapter 2

Theory of liquid crystals

2.1 The liquid crystals

Liquid crystals (LC) are a fluid state of matter composed of a collection of elongated cigar-shaped organic molecules. There are three types of liquid crystals: cholesteric, smectic and nematic [23–25]. In the case of the nematic liquid crystals, the position of the molecules are random, but their orientation tend to be the same, as shown in Figure 2.1. When a thin layer of liquid crystals is placed between two parallel glass and groved alignment layers, the molecules orient themselves in the direction of alignment layers [26–28].

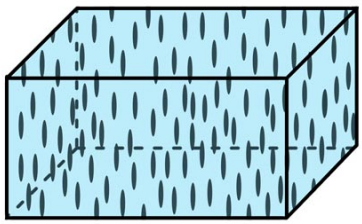

Figure 2.1: The orientation of organic molecules in nematic liquid crystals.

The change in polarization state of light caused by liquid crystals is determined by orientation of the elongated cigar-shape molecules. The orientation of the molecules can be changed of use of an electric field. Liquid crystals with alignment layers and with electrodes are called liquid crystal cells (LCc). The changing of angle between the molecules and alignment layers with applied electric field is typical for nematic and twisted nematic liquid crystal cell and vertically aligned cell (VA), or can be constant and changes of polarization output states

are achieved by rotating of the molecules in the cell axis, which is called in-plane switching (IPS) [29].

Twisted nematic liquid crystal cell (TN LCc) are nematic liquid crystals cell with crossed alignment layers [24, 30]. Without applied voltage on electrodes, molecules have a twisted structure (Figure 2.2), with applied voltage, the tilt angle (angle between the glass plate and molecules) starts increasing and finally, the molecules take a position as shown in Figure 2.3. After the electric field is switched off, the helical structure is again restored by the alignment layers.

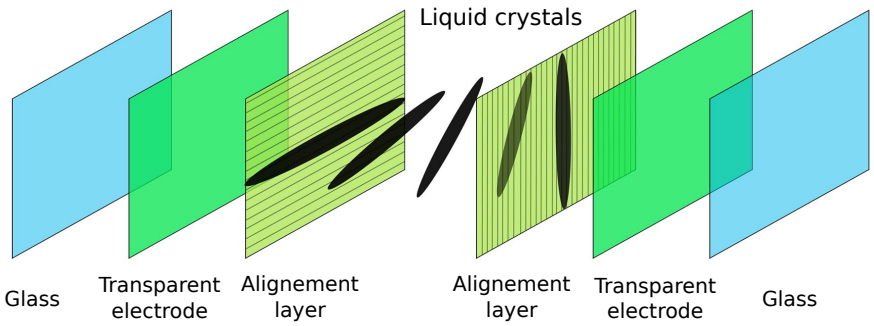

Figure 2.2: Structure of twisted nematic liquid crystal cell without the applied voltage on electrodes.

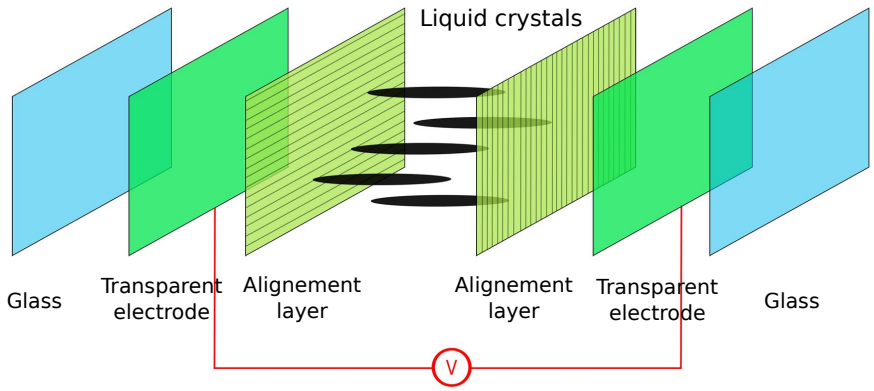

Figure 2.3: Structure of twisted nematic liquid crystal cell with the applied voltage on electrodes.

Liquid crystals must be controled by alternating current (AC) voltage. Applying a direct current (DC) voltage brings a change of chemical composition due to selective adsorption of ions. Thus DC can cause damage to the liquid

cell [31]. Therefore, it is important to ensure that the control signal has a zero DC component.

A typical control signal for twisted nematic liquid crystal cell is shown in Figure 2.5. For simplicity, all the voltages mentioned in this work in relation to liquid crystals cells and device are referred to as peak-to-peak voltage values.

2.1.1 Liquid crystal dislay

Liquid crystals find considerable use in imaging technologies as liquid crystal display (LCD). LC displays are one of the most widely used technologies for the production of liquid crystal displays [29, 32]. Nowadays the LC displays are often created from the IPS cells because of its better viewing angle. But TN LC displays are still commonly used in displays with high resolution and high refresh frequency or in simple devices like calculators for its price. TN LC display can be created from TN LC cell as follows, TN LC cell is covered with linear polarizers, mirror reflective layer, and protective layers. The typical structure of the TN LC display is shown in Figure 2.4. Thus, the TN LC cell can be made of any TN LC display by cleaning it of unnecessary layers.

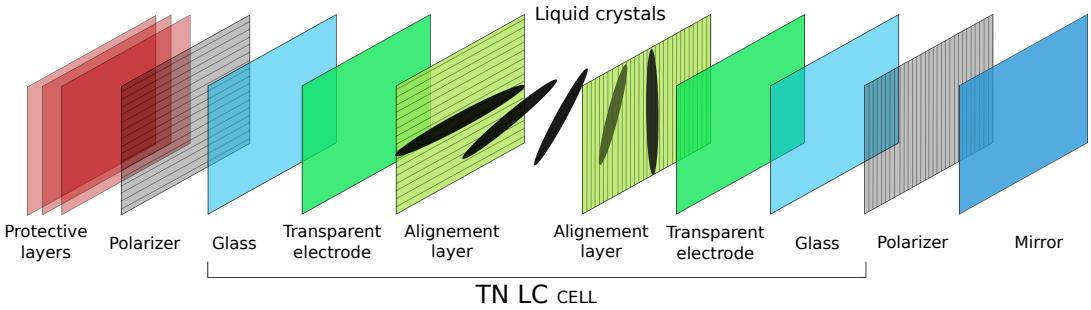

Figure 2.4: The usual structure of monochromatic twisted nematic liquid crystal displays without backlight which using reflection.

2.2 Modeling twisted nematic liquid crystals

2.2.1 Derivation of Jones matrix of the TN LC

Jones calculus can be used for description of polarization transformation of twisted nematic liquid crystal cell. The transformation matrix of the TN LC cell can be derived as a sequence of infinitesimal phase plates, each them rotated by an infinitesimal angle [33, 34]. The finally TN LC cell matrix has a form:

$$M_{\mathrm{TNLC}} = \lim_{N\to\infty} \left\{ \prod_{m=1}^{N} R(-m\varrho) \begin{pmatrix} e^{\frac{-i\delta}{N}} & 0 \\ 0 & e^{\frac{i\delta}{N}} \end{pmatrix} R(m\varrho) \right\}$$
$$= R(\varphi) \begin{pmatrix} \cos\chi + i\frac{\delta}{\chi}\sin\chi & -\frac{\varphi}{\chi}\sin\chi \\ \frac{\varphi}{\chi}\sin\chi & \cos\chi - i\frac{\delta}{\chi}\sin\chi \end{pmatrix}, \tag{2.1}$$

where φ is fixed twist angle, δ represents the phase delay dependent on the applied voltage,

$$\chi = \sqrt{\varphi^2 + \delta^2}, \tag{2.2}$$

and $R(\varphi)$ is the rotation matrix

$$R(\varphi) \quad = \begin{pmatrix} \cos\varphi & \sin\varphi \\ -\sin\varphi & \cos\varphi \end{pmatrix}. \tag{2.3}$$

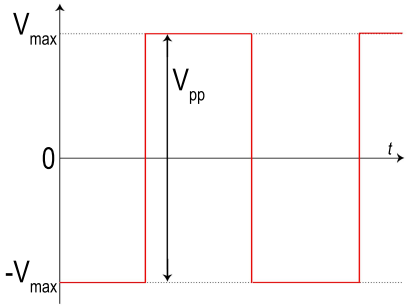

Figure 2.5: Control signal for twisted nematic liquid crystall cell. V_{max} - amplitude of AC voltage, V_{pp} - peak-to-peak voltage.

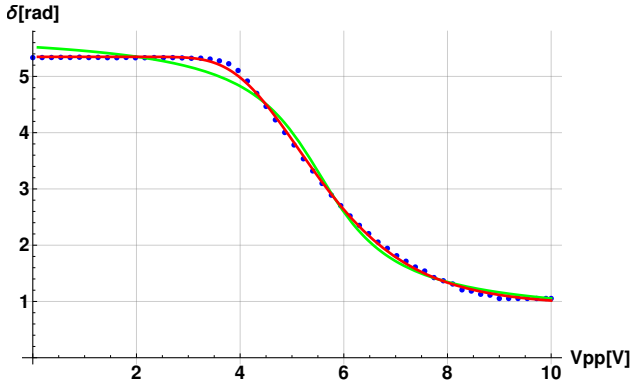

Figure 2.6: Phase delay depending on the applied voltage. Blue dots - measured data for LUMEX LCD-S101D14TR. The arctan function is represented by green curve and logistic function (2.4) is represented by red curve. For both functions I made fit for LUMEX cell data.

The phase delay is constant for the low voltage applied on the TN LC cell, after exceeding the threshold voltage, the phase delay is decreasing nonlinearly. Arctan function is often used to approximate phase delay of TN LC cell [35], but this description is not accurate (see Figure 2.6). Therefore, it was useful to find a description that would help to improve the TN LC cell model and better

approximate the phase delay behavior. The logistic function has proven to be a good approximation,

$$\delta = \alpha + \frac{1}{\beta + e^{\gamma - \delta V^{\omega}}}, \tag{2.4}$$

where α, β, γ, δ, and ω are constants and V is voltage applied on module.

2.2.2 Model issues and possible solutions

Although the basic analytical model has been improved by the more accurate description of the phase delay dependence on voltage, the match of the actual measured data with the model is not sufficient to directly determine the TN LC cell output state given to the applied voltage (see section 2.2.3). In the model described above, the distribution of the twist has constant derivation through the cell. The tilt angle is changed by an applied electric field, but it has a constant value in the whole cell, as shown in Figure 2.7a. However, this description does not correspond to the real behavior of the TN LC cell when the twist and tilt angles vary along the cell axis, their value is varied with the distance from the alignment layers. The TN LC cell can be divided into three [36, 37] or more sub-layers [37] for a better description. In each sub-layer, the twist angle behaves linearly and the tilt angle is constant, see Figures 2.7b and 2.7c.

The TN LC cell causes a small residual change of polarization state even for an arbitrarily high allowed voltage applied on electrodes. This is because of the layers near the alignment layers slightly react to the electric field in TN LC cell and cause small polarization change. Therefore, it is impossible to take away the influence of TN LC cell using applied voltage.

Even though the description in equation (2.1) is one of the simplest mathematic descriptions of TN LC cell, this model cannot be inverted and, for the desired output polarization state of the light, the voltage applied to the TN LC cell cannot be directly estimated.

Unfortunately, even advanced models do not cover all the phenomena that may occur in TN LC cells. I encountered the problem of weak depolarization while using TN LC cells. This phenomenon may be accompanied by polarization-dependent losses and these effects must be taken into account when working with TN LC cells. For TN LC cells which we use, it is possible to observe the decrease of purity with increasing the number of the cells, for one TN LC cell the average purity is 0.993(9) and for three cells it is 0.977(9).

Depolarization is often caused by the multiple-beam reflection in the TN LC cell [38]. This effect is caused by a difference of refractive index of ITO electrodes [39], alignment layers, glass plates, and liquid crystals [40]. The state of

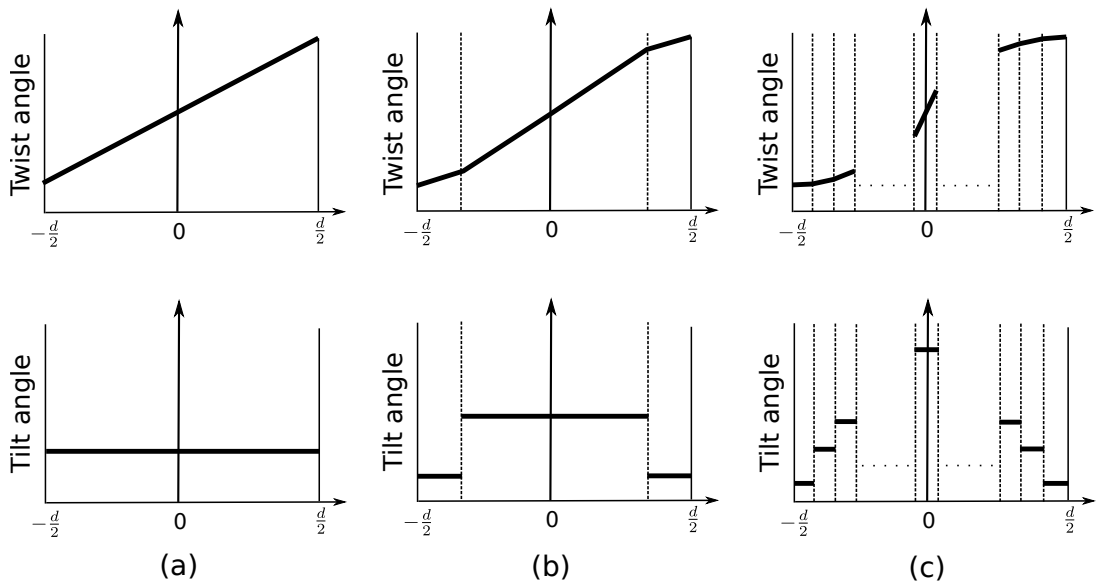

Figure 2.7: Comparison of a possible models of TN LC cells [37], basic model (a), three-layers model (b) and multiple layers model (c).

polarization of the beam without reflection in the TN LC cell is, in general, different from the state of polarization of the beam with multiple reflections in TN LC cell. These two differently polarized beams are subsequently incoherently added to the transmitted beam. However, the output beam does not have to be composed only of multiple beam reflections in the TN LC cell, but each part of it may have a different polarization depending on the non-homogeneous thickness of the LC layer. These effects can cause beam depolarization. The second phenomenon is interference between the waves passing through the TN LC cell straightly and waves that most often comes into being from the multiple reflections in the layers surrounding the TN LC layer. These layers are significantly thinner than the TN LC layer and there is mutual interference. This multiple-beam interference appears as relatively fast oscillations and in a real experiment can be smoothed due to the finite resolution of detectors [38]. These effects typically depend on the position of the beam, mechanical construction of the TN LC cell and on an applied voltage on electrodes.

The problems are expected to be minimized using custom high-precision anti-reflection-coated TN LC cells. I have tried several sources with different coherence lengths. The different coherence length had almost no effect on the purity of the reconstructed state. Therefore, I believe that, in the case of TN LC cell, interference phenomena are not the dominant source of depolarization.

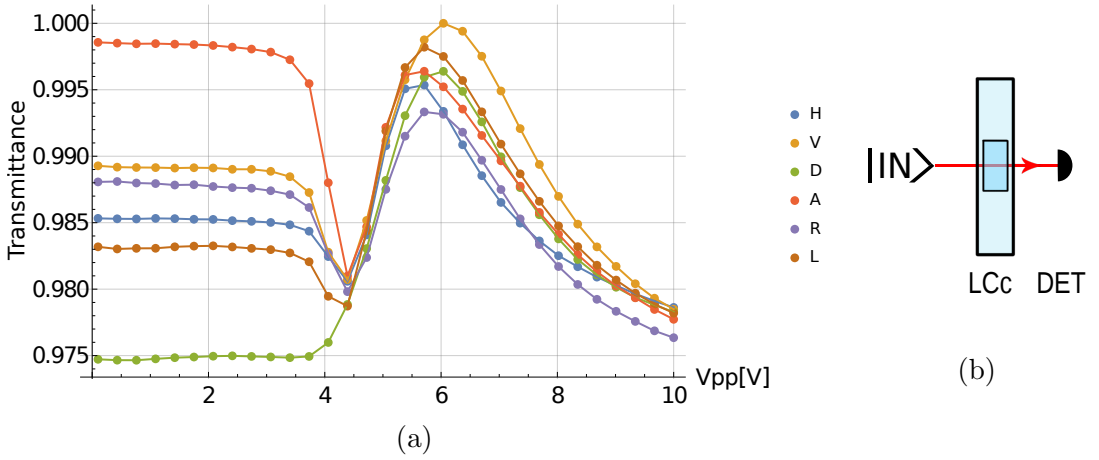

(a) (b)

Figure 2.8: Measured polarization-dependent loss for TN LC cell from LUMEX LCD-S101D14TR. (a) Measured transmitance for applied voltage on the TN LC cell (LCc) in the range of 0.1-10V_{PP} and various input states of polarization (horizontal (H), vertical (V), diagonal (D), anti-diagonal (A), right (R) and left (L) circular polarization). (b) The scheme of setup that was used to analyze polarization dependent losses, $|IN\rangle$ represents different input states of polarization.

In addition to this, we can also observe changes in transmitted intensity behind the TN LC cell. Output intensity typically varies with the state of polarization of the input beam and orientation of LC molecules in the cell affected by the applied voltage. In Figure 2.8a I show the results of a measured polarization dependent loss for TN LC cell and its dependence on the applied voltage to electrodes. Changes in the detected intensity are quite small, but these changes may affect the output state, especially when multiple cells are used. Figure 2.8b shows the experimental scheme that was used for polarization-dependent loss analysis. As can be seen in Figure 2.8a, for the 0-4V voltage range, the differences between the polarization states are greatest. Taking into account the progress of retardation (see Figure 2.6), where the retardance is almost unchanged in the 0-4V range, it is advisable to limit the range of suitable voltages. For these reasons, it is recommended to operate the TN LC device in the 4-10V control voltage range for each TN LC cell.

The problems like depolarization and others are not covered in any model mentioned above, and it is hard to build the analytical model of TN LC cell including all these effects. One of the ways how to solve this issue is to use machine learning. Machine learning uses an artificial network of neurons to predict outcomes by learning the model from acquired data.This artificial network is used to build the algorithm that can receive input data and compare them with known

outputs to learn the artificial network and improve the prediction accuracy of outputs. Machine learning can not only improve the accuracy of prediction of the polarization state at the output of a TN LC cell for a particular applied voltage but also allows to predict the voltage required for the target polarization transformation.

2.2.3 Comparison of real data with model

As mentioned above, the analytical model, especially the basic model following equation (2.1), does not agree with the results actually measured, see Figure 2.9a for single TN LC cell and Figure 2.10a for TN LC device made from three TN LC cells. For comparison, I use a mean absolute error,

$$\mathrm{MAE} = \frac{\sum_{i=1}^{n} |y_i - x_i|}{n}, \tag{2.5}$$

where x_i represents predicted Stokes parameter, y_i represents measured Stokes parameter, and n is the number of Stokes parameters in the dataset.

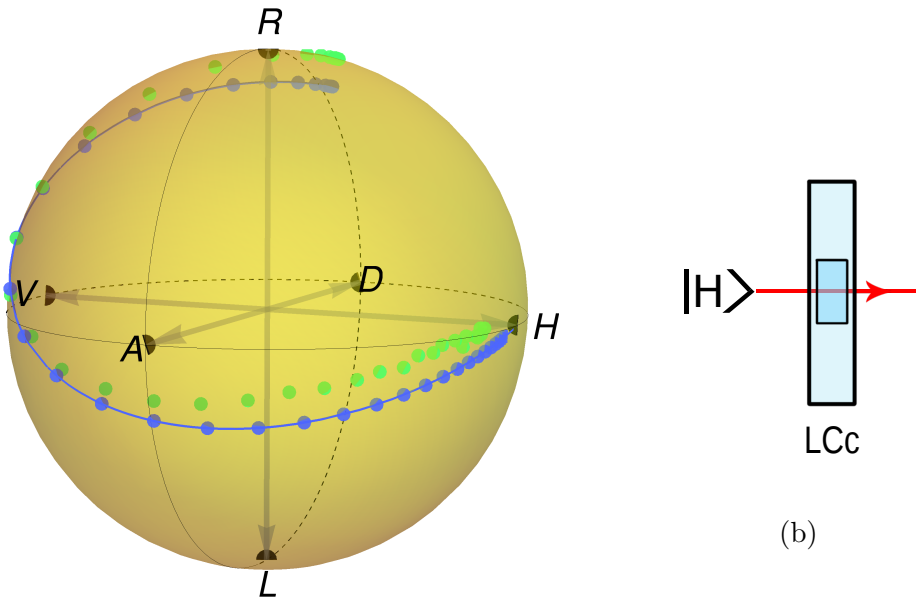

(a) (b)

Figure 2.9: Comparison of the trajectory on the Bloch sphere (a) for the basic model (blue) and measured states (green dost) for 1x TN LC cell (LCc). 1x TN LC cell (b) configurations used for computing MAE.

I evaluated MAE for two cases, one TN LC cell (Figure 2.9b) and three TN LC cells placed one after the other (Figure 2.10b). To illustrate the benefits of deep learning, I also demonstrate the value of MAE for the polarization transformation prediction for the three TN LC cell side by side acquired with experiment, the basic model and with the model based on machine learning. For MAE evaluation, I used H polarization as an input to TN LC cells and different voltages were applied to individual cells. In this way, more than 20,000 data was acquired to train the machine learning model and for evaluating MAE. The same data were used for evaluating MAE of the basic analytical model. The small discrepancy between the application of the basic analytical model to single TN LC cell and three TN LC cells is caused by the higher purity of the states prepared by the single TN LC cell. The increasing of the number of TN LC cells brings purity losing, as I already discussed in the previous section. And because of only fully pure states are predicted by the basic analytical model, the MAE value for the basic model decrease with the purity of real prepared states. The results for the basic model and benefits of machine learning can be seen in the Table 2.1. For correct comparison, the accuracy of the machine learning model was evaluated on a different set of data than the one on which the model was trained.

It is hard to illustrate the differences between the basic analytical model and machine learning model if all cells voltage varies. For visualization in Figure 2.10a, I fix the voltage on the first and second TN LC cell and only the third cells voltage is changing.

	1x TN LC cell	3x TN LC cells	
	Basic model	Basic model	Machine learning
MAE	0.128	0.122	0.004

Table 2.1: Mean absolute error (MAE) for the basic model and for model acquired by machine learning and for different configurations of TN LC cells.

I would like to thank Dominik Vašinka for creating the machine learning model of the TN LC device. The used methods and obtained results will be described in detail in his upcoming bachelor thesis [41].

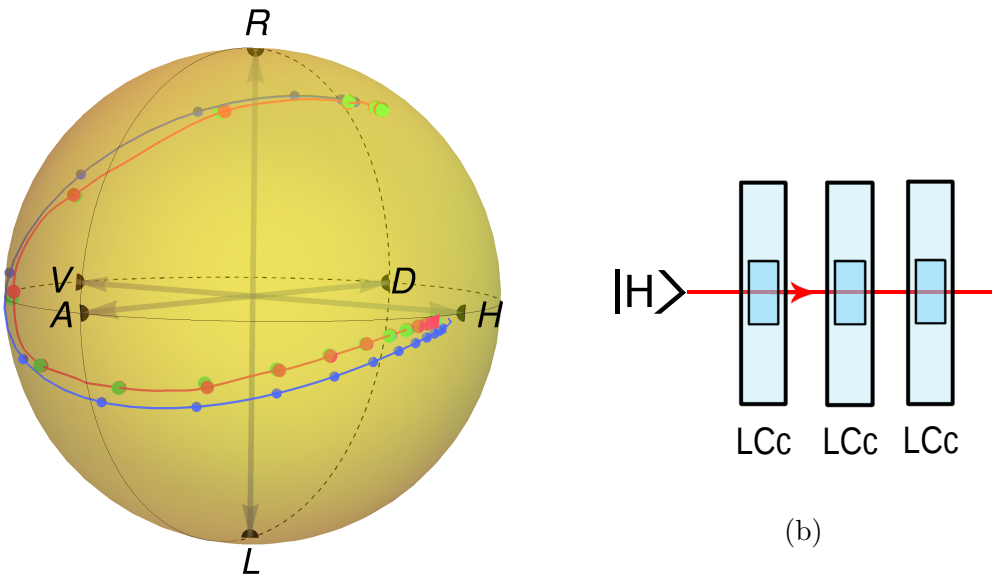

(a) (b)

Figure 2.10: Comparison of the trajectory on the Bloch sphere (a) for the basic model (blue), deep learning model (red) and measured states (green dots) for 3x TN LC cell (LCc). (b) Configuration with three equally oriented TN LC cells. Voltage applied on first and second TN LC cell is constant and voltage applied on the last TN LC cell were varied.

Chapter 3

Liquid crystal polarimetry

3.1 Construction of loquid crystal device

Almost any nematic liquid crystal can be used for polarization control. The liquid crystal cell can be custom-made, or it is possible to modify a commercially available liquid crystal display. We decided to use conventional twisted nematic liquid crystal display LUMEX LCD-S101D14TR (see Figure 3.1a) to create a TN LC device (TN LCd). TN LC display is covered by polarizers and protective layers. These additional layers must be removed from the display before using it for polarimetry. The TN LC cell from the LUMEX display offers eight segments that can be individually controlled, but only one of them is used to create the TN LC device as shown in Figure 3.1b.

There are many possible configurations of the TN LC devices, consisting of various numbers of TN LC cells, wave plates, and others elements. But not all of them are suitable for the intended purpose. Some configurations do not cover the Bloch sphere sufficiently, which can be solved by a higher number of TN LC cells. On the other hand, as the number of cells increases, the complexity of the driving and the complexity of adjustment of the entire device increase. Increasing the number of TN LC cells also highlights some negative effects such as the depolarization and polarization-dependent loss.

The search for the optimal configuration was performed by numerical simulation based on the mathematical model (2.1), which had been characterized for used TN LC cell [42]. In these simulations, I searched for maximum fidelity with the H, V, D, R and L polarization. To speed up the simulation, I used a genetic algorithm. I generated random three voltages to initialize the algorithm, compute corresponding states and theirs fidelities with the target state. From this zero generation, I chose states with best fidelities and crossing them with each other. As a crossing-over method, I made use of the arithmetic mean of

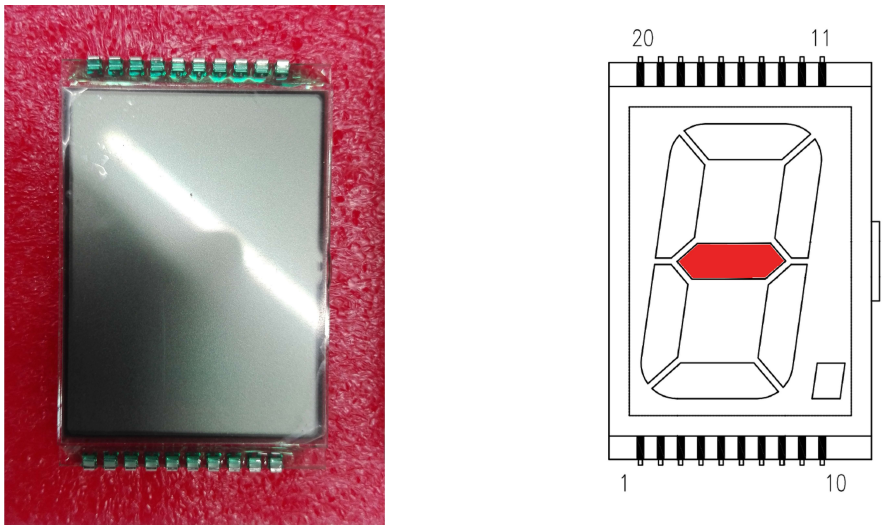

(a) (b)

Figure 3.1: The photo of used TN LC display (a) and the schematic representation of the display segments, highlighted in red is the segment used to control the polarization (b).

the corresponding voltages of the states of polarization with best fidelities and add small mutation on randomly chosen voltage component. These steps were repeated until the fidelity of states increased over 0.999. Based on these numerical simulations performed on the basic model (2.1) I select the configuration with three equally oriented TN LC cells (see Figure 3.2). This configuration offers the largest active area, it can be useful for example to control two or more parallel beams at the same time and others. This configuration offers three independent parameters, three voltages applied to the TN LC cells.

3.1.1 Calibration of the device

For precise calibration of the TN LC device, it is necessary to have some etalons of basic states of polarization. Therefore I constructed two conventional polarimetric analysis. Both of them utilized half-wave and quarter-wave plates in high-speed rotation stages PR50CC (Newport). First one was used as a polarimetric analyzer for calibration TN LC device. The setup for calibration TN LC device is shown in Figure 3.3a. The second analyzer was used for independent preparation of referenced states of polarization to compare the accuracy of the analysis with TN LC device and the commonly used wave plate polarization analysis method (see Figure 3.3b).

Because the basic mathematical model (2.1), as I mentioned above, is not

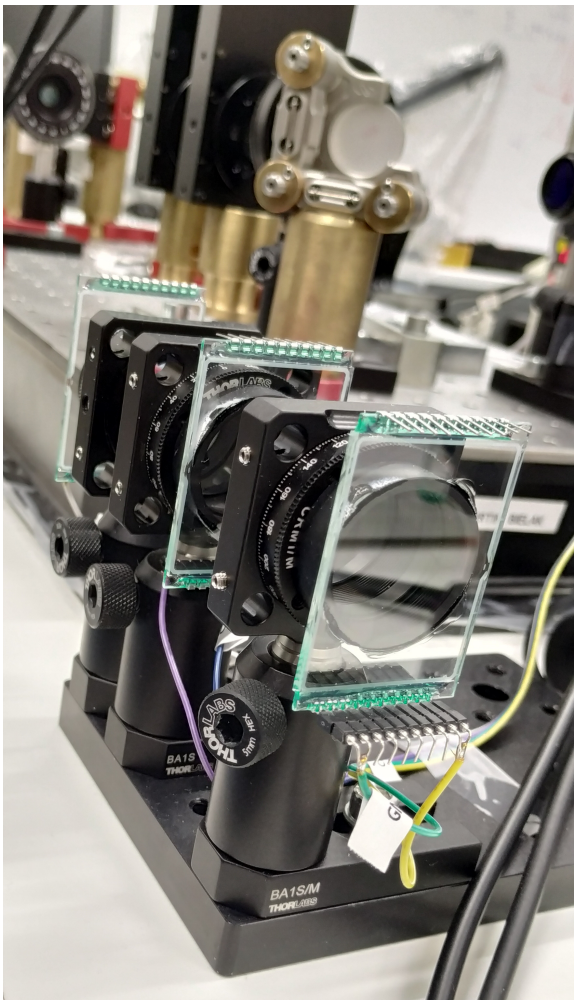

Figure 3.2: Photography of TN LC device made from three TN LC cells.

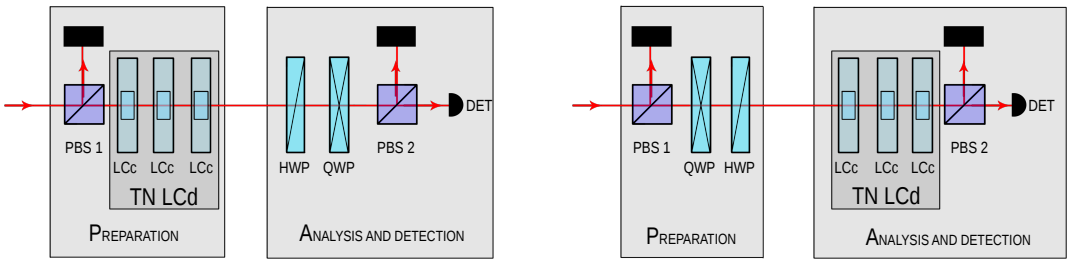

(a) Scheme used for calibration TN LC devices.

(b) Experiment scheme for verifying polarization analysis using TN LC devices.

Figure 3.3: Polarizing beam splitter (PBS), quarter-wave plate (QWP), half-wave plate (HWP), detector (DET), TN LC cell (TN LCc).

accurate, it was not possible to use only numerical simulation to look for exact voltages which must be applied on TN LC cell. Therefore, it is necessary to search for the exact values of the voltages in the experiment. As the first step, the H projection was set on the wave plates and several randomly chosen voltage triples close to the best voltages found by the simulation based on the basic mathematical model were applied to the TN LC device. By the same genetic algorithm which was used for the numerical simulation, I searched maximum output from the detector for H state and minimum for V state. This procedure was repeated for projections into the other base states D, A, R and L. After that I applied the best combinations of voltages on TN LC device and measured states prepared by TN LC device. Stokes parameters of prepared polarization states are shown in Table 3.1. States of polarization prepared by TN LC device are shown in Figure 3.4a too. I have achieved average purity 0.984(4), average fidelity 0.990(3) and an average angular deviation of 1.936 degrees, measured as the angle between the stokes vectors of the states prepared by TN LC device and corresponding ideal states. After this procedure the device is calibrated and could be used to prepare and analyze states of polarization.

Stokes parameters	State H	State V	State D	State A	State R	State L
S1	**0.979**	**-0.979**	0.014	0.061	-0.024	-0.018
S2	0.063	-0.035	**0.991**	**-0.981**	-0.125	0.020
S3	0.061	-0.018	0.027	0.063	**0.976**	**-0.980**

Table 3.1: Stokes vectors of H, V, D, A, R and L states prepared by TN LC device (measured by wave plate).

The projection into eigenstates of Pauli operators is not the only way how to analyze the polarization states. The goal was to develop the device switchable between two modes, HVDARL mode (projections to eigenstates of Pauli operators), and 4 states mode (minimal tomography [17]) without any change in HW configuration. Thus I search also for voltages and corresponding four states required for minimal tomography. Appropriate states were searched by attaching random voltages to the TN LC cels, the prepared states were reconstructed by wave plates. For minimal tomography, it is necessary to find states forming the peaks of a regular tetrahedron inscribed in the Bloch sphere to achieve a tomographic complete results [17]. There are unlimited possibilities how to inscribe tetrahedron into the unit sphere, but the TN LC device cannot cover all points

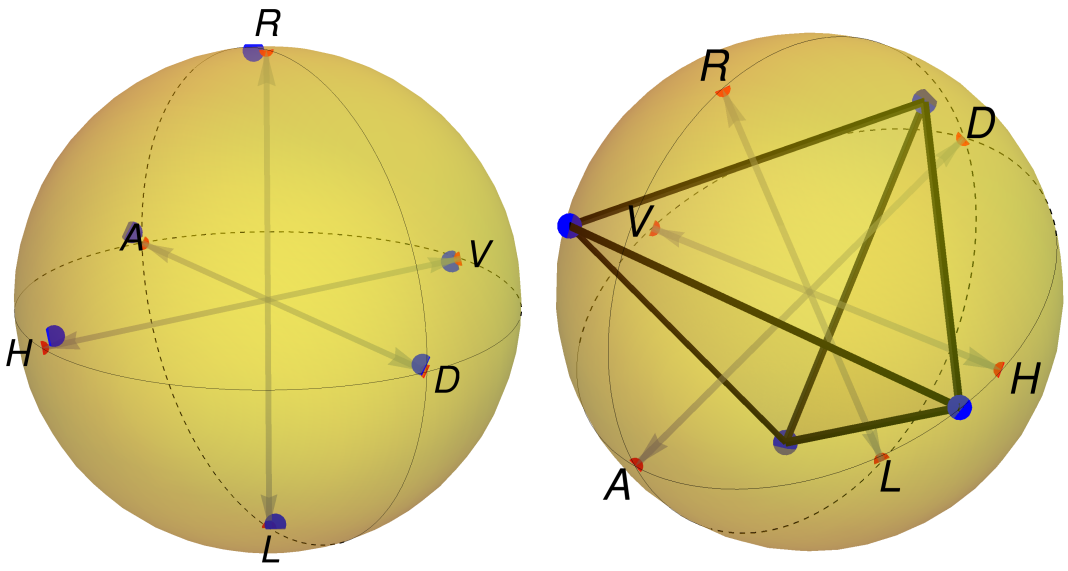

(a) (b)

Figure 3.4: Visualization of prepared states by means of TN LC device on the Bloch sphere. Red points represent ideal H, V, D, A, R and L states and blue points represent states prepared by TN LC device. Figure (a) shows prepared H, V, D, A, R and L states of polarization by TN LC device and Figure (b) shows prepared states which create nearly regular tetrahedron inscribed to the Bloch sphere.

on the Bloch sphere with the same quality because of slight depolarization and others issues. So, it is necessary to search the best 4 states that creates the vertices of the best nearly regular tetrahedron in the optimum voltage subspace. By not precisely determining the exact position of the tetrahedron peaks, it is not possible to evaluate the suitability of the individually prepared states by fidelity. Instead we utilized the fact that a regular tetrahedron inscribed in the Bloch sphere has the largest volume of all possible tetrahedrons that can be inscribed in the unit sphere. Therefore, I used a comparison using the volume of the tetrahedron, which is formed by points described by Stokes vectors in the Bloch sphere. Found states are very close to the ideal regular tetrahedron, the ratio of its volume to the regular tetrahedron written into the Bloch sphere is $V_{\text{tet}} = 0.972\ V_{\text{ideal}}$ and its Stokes parameters are shown in Table 3.2. Found tetrahedron is shown in Figure 3.4b.

Stokes parameters	ρ_1	ρ_2	ρ_3	ρ_4
S1	-0.130	-0.462	-0.383	0.968
S2	0.965	-0.576	-0.185	-0.208
S3	0.182	0.674	-0.885	-0.004

Table 3.2: Stokes vectors of tetrahedron vertices ρ_1, ρ_2, ρ_3 and ρ_4 prepared by TN LC device and measured by wave plate.

3.1.2 Ability of the device to prepare arbitrary polarization states

Mixed state preparation

In addition to almost pure polarization states, it is also beneficial to be able to prepare partially mixed states. Polarization mixed state can be prepared as a statistical ensemble of pure states. One of the techniques of effective depolarization of the beam is to temporal averaging a of the states of polarization [43]. To achieve this, it is necessary to have precise control over the device which allows quick change of prepared states during the measuring.

To demonstrate the quality and versatility of our TN LC device we decided to prepare a mixed polarization state. I quickly change polarization states H, V, D, A, R and L prepared by changing voltages applied on TN LC device during measurement output state. For reconstruction were used wave plates. TN LC device was able to prepare the state with purity 0.50005 and length of Stokes vector 0.01046.

Covering the Bloch sphere

In my bachelor thesis [42], I demonstrated accurate preparation of six polarization states from three mutually unbiased bases using two independent TN LC cells and a fixed wave plate. But this configuration of the device may not be sufficient and sometimes it is necessary to prepare any state on the Bloch sphere or in its volume. The method of preparing the state in the Bloch sphere was described in the previous section.

The developed three-TN LC-cell device was emlpoyed to prepare an arbitary state of polarization. The device was tested for more than 20,000 combinations of three control voltages, each of them ranging equidistantly from 0 to 10 V. The corresponding output state of polarization was measured by a reference polarimeter

based on rotating wave plates. Measured states of polarization and Bloch sphere coverage are shown in Figure 3.5. Bloch sphere is not covered evenly, this is due to the non-linear dependence of retardance on the applied voltages on TN LC cell (see Figure 2.6). To quantify the coverage of the Bloch sphere by the prepared states, I calculated the radius of a sphere, which contains just one measurement result, for all the prepared states. The average radius of such sphere is 0.01(1) and the maximum radius is 0.12. I assume that these values are mainly limited by the used sampling of voltages. For a finer division of the applied voltage interval, I expect a decrease in this value. These measured state of polarization were also used for building the deep learning models [41].

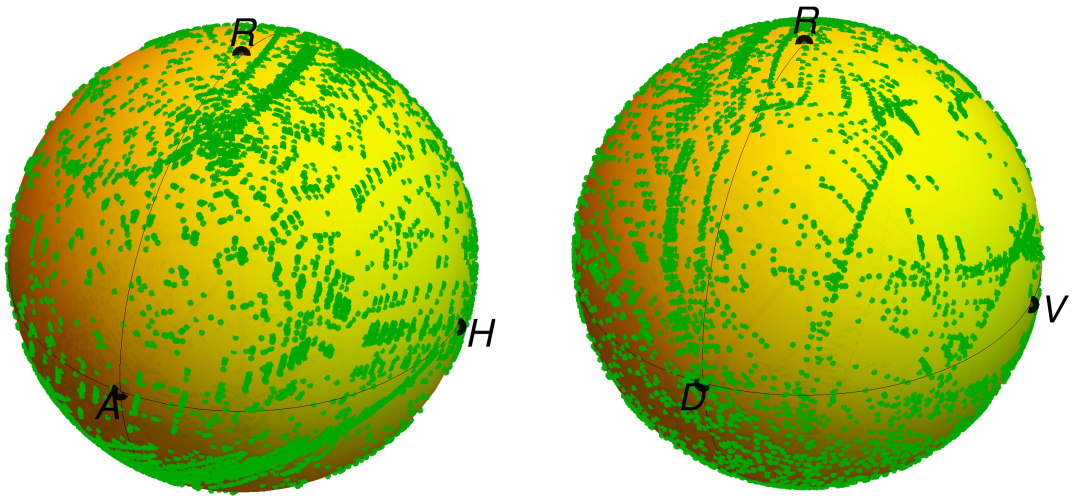

Figure 3.5: Coverage of the Bloch sphere of TN LC device, green points represent states of polarization prepared by TN LC device made from three TN LC cells. Bloch sphere is not covered evenly, this is due to the non-linear voltage dependence of TN LC retardance.

3.2 Twisted nematic liquid crystal device as polarimetry analyzer

In this case, I tested the TN LC device made from three TN LC cells as a polarimetric analyzer. In order to evaluate the quality of the polarization analysis, it is necessary to analyze several states, as the analysis can be differently accurate for different polarization input states. That is why I decided to test the

TN equipment for the analysis of three pairs of mutually unbaised states of polarization, namely the horizontal, vertical, diagonal, antidiagonal, right-handed and left-handed circular polarization. The states were prepared by wave plates and measured by TN LC device, the experimental setup was similar as in Figure 3.3b. Required projections were sequentially set on the TN LC device and the data were subsequently evaluated using maximum likelihood [44]. I used the projections to eigenstates of Pauli operators (HVDARL mode) and, also, the minimal tomography.

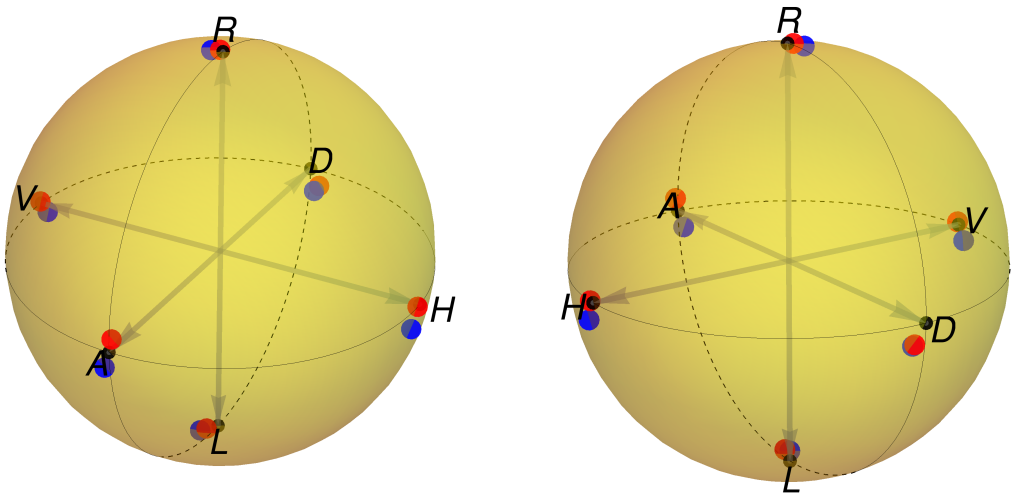

Figure 3.6: Measured states of polarization prepared by wave plates and measured by the TN LC device in booth polarization analysis modes. On the Bloch sphere are shown states measured by the TN LC device in HVDARL mode by red dots, the blue dots represent states measured in 4 state mode of TN LC device.

Stokes parameters of states measured by TN LC device are shown in Table 3.3 using projections to eigenstates of Pauli operators and in Table 3.4 using the minimal tomography. A comparison of two methods employing TN LC device and its analysis using wave plates is shown in Table 3.5 and in Figure 3.6. In the case of the analysis using projections to eigenstates of Pauli operators, the left-hand circular polarization has lower purity than other reconstructed states. The measurement was repeated with the similar result. We do not know yet the reason for this selective purity drop. Maybe it is caused by using the voltage for third TN LC cell at the edge of an appropriate range or it comes from some other TN LC cells phenomena. For future use of the device, it is necessary to study this issue further.

It is important to stress that the discrepancies between observed and the

corresponding ideal states arise not only from the analyzer imperfection but it is also caused by nonideal state preparation. The 4-state minimum tomography gives on average worse results than 6-state HVDARL analysis. This may be due to the greater sensitivity of the four state space to the present systematic errors. The same wave plates were used for both methods of analysis.

Stokes parameters	State H	State V	State D	State A	State R	State L
S1	**0.9996**	**-0.9999**	0.053	0.013	-0.021	-0.023
S2	-0.027	-0.008	**0.995**	**-0.998**	0.14	-0.078
S3	0.001	0.013	-0.085	0.067	**0.9997**	**-0.970**

Table 3.3: Stokes vectors of H, V, D, A, R and L states of polarization prepared by wave plates and measured by TN LC device in HVDARL mode.

Stokes parameters	State H	State V	State D	State A	State R	State L
S1	**0.991**	**-0.997**	0.040	-0.028	-0.071	-0.056
S2	-0.063	0.046	**0.964**	**-0.994**	0.025	-0.085
S3	-0.098	-0.070	-0.103	-0.089	**0.984**	**-0.994**

Table 3.4: Stokes vectors of H, V, D, A, R and L states of polarization prepared by wave plates and measured by TN LC device using 4-state tomography.

These results may not seem very convincing at first glance. In direct comparison (see Table 3.5), analysis using wave plates gives slightly better results. However, in more complex experiments with a lot of other components and more analyzed modes of light, these slight differences are not essential. In these complex experiments, purity often decreases below 0.90 even when accurate wave platelets analyses are used. If a TN LC device is used, we can state the errors of the TN LC device are much smaller than the typical repeatability of such complex experiments. As I pointed out in my previous thesis [42] on the example of reconstruction of GHZ (Greenberger–Horne–Zeilinger) state [45, 46], we are not able to tell whether the results with analysis by TN LC devices are better or worse. We can conclude that analysis using the TN LC device gives results compatible with wave plate analysis.

Used analysis method	TN LC device		Wave plates
	HVDARL	4 states	HVDARL
Purity	0.997(8)	0.99(1)	0.9994(7)
Fidelity	0.997(5)	0.994(6)	0.9994(5)
Deviation [°]	$15(10)\times10^{-1}$	2.8(5)	1.1(4)

Table 3.5: Achieved average results of purity, fidelity and angular deviation between measured H, V, D, A, R, L states of polarization and the corresponding ideal states. The states were prepared by wave plates and measured by TN LC device in both tomographic modes and by another wave plates.

3.2.1 Time response of projection settings

One of the advantages of using liquid crystals in the preparation and analysis of states of polarization is the rate of setting projection to the desired states. When one polarization state is analyzed it is necessary to make 4 or more projections. For each projection, it is necessary to change the applied voltage in case of TN LC device or change the angle of rotation of a wave plate. However, the transitions between the individual projections take different time. Notwithstanding, it does not matter on the sequence of these projections, so it is appropriate to look for such a sequence of projections for which the total analysis time reaches its minimum.

Typically, the transition time between the desired states of TN LC cell depends on many factors. These factors include LC layer thickness, a viscosity of crystals, temperature, or difference of applied voltage. In general, the LC cell response time is much faster when using higher values in the electric field [47]. The response time is also dependent on the direction of change in retardation as well as the absolute required value of the retardation of the LC cell.

For this measurement, it can be used the setup which is shown in Fig. 3.3b with small modifications. Firstly A/D converter was connected to the detector output and the time between changing the voltages applied to the TN LC modules and value stabilization from the A/D converter were measured. Because it is necessary to set the same conditions for all measurements, as the initial state at the beginning of each sequence of projections, I use voltage 0V applied to all cells. I did this measurement for an older version of the LC device that was made up of a pair of TN LC cells and HWP. Since the application of voltage is parallel and always dependent on the slowest change, it is no matter the number of cells, the total number of cells does not affect the total time. The total time required for

the change of projection depends on the differences between the applied voltage before the change and on the target voltage. Based on this and the experience of using the TN LC device in experiments, the values given in Table 3 for the older TN LC devices can be considered as orderly corresponding for the current version of the device. For the TN LC device, I measured all sequences of projection. The resulting data were processed and the results are shown in Table 3.6. For comparison, I also measured some sequences of projections for wave plates in high-speed rotation stages PR50CC (Newport).

Used analysis method		Min	Max	Average	Med
TN LC device	HVDARL	4,48 s	8,80 s	6,00 s	5,93 s
	4 states	3,54 s	6,64 s	4,47 s	3,99 s
High-speed rotation stages		27,90 s	42,77 s	32,89 s	32,43 s

Table 3.6: Total analysis time for one input state of polarization.

When the best sequence of projections is used, the analysis time by TN LC devices can be up to 8 times faster than in case of use high-speed rotation stages and wave plates.

Chapter 4

Comparison of tomographic schemes

The main problem of quantum state estimation is to find the most efficient measurement and data processing framework so that the quantum state is determined as accurately as possible. Quantum estimation is a procedure used to derive a quantum system state from generalized measurements [44]. Typically with the increasing number of the dimension the total time required to analyze one quantum state rapidly increases. In common experiments, the possible measurements are determined by the experimental setting, which can not be easily changed. The simplest measurement scheme consists of the same and independent measurements on a set of identical copies of quantum states.

The measurement is called information complete measurement if the quantum system measurement allows estimating the operator's expected value only from measurement statistics [48]. In the case of a single qubit, the minimal tomography [17] is a example of information complete measurement, it has exactly four outputss. If the measurement has more outputs, these measurements are called information overcomplete measurement. A prominent example of these measurements is a complete set of mutually unbiased bases. For one qubit the measurement by projection onto the mutually unbiased base is similar to the projections to eigenstates of Pauli operators [19], for a higher dimension, the mutually unbiased bases are difficult to achieve in polarization tomography because it includes projections onto entangled states [49]. Another example of the information overcomplete measurement is a covariant measurement [20–22, 50].

It is right to ask what kind of measurement is the most effective and leads to the best estimation of the state of polarization. The accuracy of the information complete measurements and some information overcomplete measurements have already been shown theoretically in the literature [17, 20, 49, 51, 52].

To test tomographic methods, it is necessary to prepare a large number of input states of polarization randomly distributed over the state domain, because the chosen estimation method may favor some input states. Subsequently, these states need to be analyzed by a set of projections. The TN LC device is perfectly suited for testing and comparing individual quantum state tomography methods because TN LC device allows preparing a large number of polarization states and allows switching quickly between them. Likewise, the TN LC device enables a large number of projections to be prepared for analyzation too. Unfortunately, there is currently only one TN LC device available to allows preparing any projection. Therefore, in this chapter, I will only deal with the simulation of the experimental use of the TN LC device and the design of the experimental setup for subsequent verification.

4.1 Experimental setup design

As I have already indicated, it is necessary to use two TN LC devices for experimental verification. Use of wave plates would significantly increase the time required for such an experiment.

The limit of the infinite number of photons is usually considered in theoretical works. Unfortunately, this cannot be achieved in the experiment. Therefore, it is necessary to count the individual photons that are used in the experiment and to distinguish them from the dark detections. That is why I designed the experiment with a photon pairs source where one photon is used to prepare the desired state and the other serves as a triggering. In the lower arm, the polarization state is prepared using a TN LC device and subsequently analyzed using a second TN LC device. For the analysis, I used a projection onto six eigenstates of Pauli operators, or onto sixty states randomly but evenly spaced on the Bloch sphere. These requirements are reflected in the experimental layout in Figure 4.1.

4.2 Simulation of different types of tomography

To compare the results, it is necessary to define a metric for comparison accuracy of the tomography procedures. I used mean square error

$$\mathrm{MSE} = E(||\Delta\rho||^2_{\mathrm{HS}}), \tag{4.1}$$

where $\Delta\rho$ is the difference between true state and acquired state.

The minimum value of MSE for individual tomography methods has been theoretically studied [20]. For minimal tomography, the minimum value of MSE

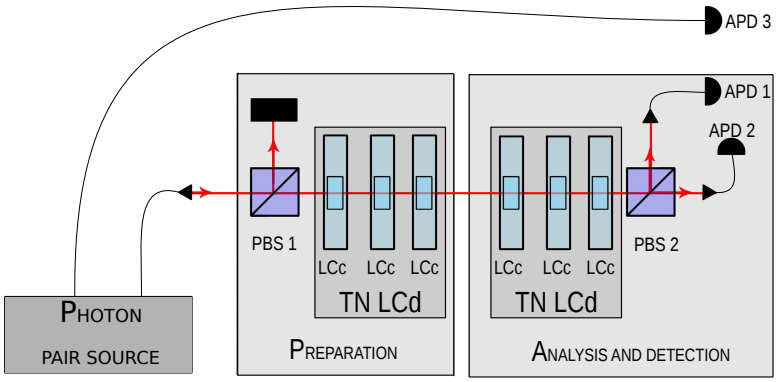

Figure 4.1: The proposed form of the experiment with two TN LC device (TN LCd) each one made from three TN LC cells (LCc). Setup using both outputs from second polarization beam spliter (PBS 2) and three avalanche photodiodes (APD).

is given by

$$\mathrm{MSE}_{\mathrm{min}} \leq d^2 + d - 1 - \mathrm{tr}(\rho^2), \tag{4.2}$$

where d is dimension of space and ρ is density matrix of measured state. For one qubit $d = 2$. For mutually unbiased bases the minimum value of MSE is given by

$$\mathrm{MSE}_{\mathrm{MUB}} \leq (d+1)[d - \mathrm{tr}(\rho^2)]. \tag{4.3}$$

As the number of projections increases, the MSE value further decreases and for covariant measurements and one qubit reaches a minimum value

$$\mathrm{MSE}_{\mathrm{COV}} \leq 2. \tag{4.4}$$

Due to the selected experimental scheme, it is not possible to perform a simulation for minimal tomography, since both polarization beam splitter outputs are used. That's why I made a simulation for six eigenstates of Pauli operators and for sixty states randomly but evenly spaced on the Bloch sphere. TN LC device would allow preparing many more projections, but the total measurement time, which is growing rapidly with the number of projections, should be taken into account. For the same reason, only a limited number of polarization input states are used. All of these measuremnts that have to be taken lead to an increase of MSE, but we expect that the MSE ratios between the individual tomographic methods will be maintained.

4.2.1 Simulation results

In order to maintain a reasonable duration of the experiment, I selected 250 different polarization input states spaced evenly across the Bloch sphere. The total number of photons on one prepared polarization state was chosen as 480. Many possible combinations have been tried, but it was proven that these values were appropriate to the total number of projections needed and thus the expected time of the experiment. The tomography of these prepared polarization states was performed by successive projections on a TN LC device. In the experiment, the infinite number of the projectors is unreachable, thus we cannot perform the covariant measurement exactly. For an approximation of the covariate measurements, I used sixty projectors. The TN LC device allows increasing the number of projectors, but the required time is rising rapidly. The polarization state was subsequently reconstructed using the maximum likelihood of the number of detected photons. Photons countings are considered in the coincidence basis of both arms.

I did the simulation for ideal projectors and for TN LC device projectors. However, even if ideal projectors are used, inaccuracies resulting from the finite number of photons and their probability distributions between the two output detectors are introduced. The comparison of the results of the simulations are shown in Table 4.1. For the simulation, I used pure states as target states. Since the maximum likelihood estimation was used in the simulation to reconstruct the polarization states, the results may be biased. We assume that this is the reason why the values of the MSE for ideal projections decrease under the theoretical limit. For this reason, it is not possible to directly compare the exact values of the MSE, but it is necessary to focus on the ratios between the different methods.

By comparing the values from the simulations, a significant improvement in the accuracy of the reconstruction can be seen. On the one hand, an increase in the number of used projectors results in a significant reduction of the value of the MSE. On the other hand, the time-consuming of such analysis is growing.

In this experiment, 250 different polarization states need to be prepared. Each prepared input polarization state needs to be analyzed with six or sixty projections. Thus, in the first case, 1500 of voltage changes on TN LC devices are required, in the second one 15000 of voltage changes. Due to the typical time of projection preparation by changing voltage and data acquisition, we assume that the total required time to perform the experiment will be 5 hours.

Also very important is the assumption of a constant number of photons per one analyzed input state. After many simulations and tried values, I finally set the total number of photons per input polarization state to 480 photons. This

Number of projectors	MSE		
	Ideal projectors	TN LC device	Theoretical (∞ photons)
4	3.2(3)	/	4
6	2.4(2)	9.3(6)	3
60	2.1(2)	5.4(2)	/
Covariant	/	/	2
Ratio	0.88	0.59	0.67

Table 4.1: The mean square error values (MSE) for different analysis methods, 480 photons per one input states and 250 input states of polarization. The last column gives the values obtained from the theoretical derivation without the influence of the used reconstruction method [20]. In the case of the measurement simulation according to the diagram in Figure 4.1, the MSE absolute value can be influenced by the reconstruction inaccuracies. The last line shows the ratio of MSE for six projectors and sixty projectors. For theoretical results, the ratio between six projectors and covariant measurements is presented.

value is achievable in the experiment and gives consistent results in simulations. A constant number of input photons means that with the increasing number of projections in the analysis, the number of photons per projection decreases. Despite the decreasing number of photons per individual projection, the simulations show a positive effect of the increasing number of projections.

Chapter 5

Conclusions and outlook

The aim of this work was to study the behavior of TN LC cells and their possible use in experiments containing analysis and preparation of polarization states. The description of polarization change caused by a TN LC cell is a complex task, particularly to derive an analytical model of the cell. In the thesis, I show several possible descriptions of the TN LC cell from the point of view of polarization. In addition to the basic model, the thesis contains a description of extended models which include some specific behavior of the TN LC cells. These extended models describe weak response of the liquid crystals near the alignment layers, but they do not describe all of the discrepancies that can occur. These models usually do not include the depolarization or polarization-dependence losses. It is appropriate to have a well-matched model with the true behavior of the TN LC cell, the solution might be to use machine learning instead of analytical models. The machine learning also allows creating an inverse model for future use. Machine learning models bring large improvement to the prediction accuracy of polarization output states. In the case of the device composed of three TN LC cells the analytical model gives MAE = 0.122 and the machine learning model reduces the MAE value to 0.004.

The thesis describes the procedure for the modification of the 8-segment LUMEX LCD-S101D14TR display for the use in optical experiments and the basic principles of its control. Surprisingly the TN LC cell from the commercially available TN LC display manufactured with low precision and without anti-reflective layers performs nicely and provides highly accurate polarization controller. The thesis describes the developing of a TN LC device consisting of three TN LC cells and its practical use in experiments. Furthermore, the thesis suggests a possible use of the TN LC device for increasing the accuracy of polarization analysis and its speedup.

The TN LC device composed of three TN LC cells was constructed based on

numerical simulations using the genetic algorithm. Necessary measurements were carried out for the use of this device in the many different types of tomography, mainly the minimal tomography and in the analysis by means of projection onto the eigenstates of Pauli operators. The aim of these measurements was to go through the voltage subspace of the TN LC device and find suitable voltage combinations for the target projections. The suitable projections for the use of the device in minimal tomography and in the analysis by means of projection into the eigenstates of Pauli operators are presented in section 3.1.1.

This device has been verified in polarization analysis too. These measurements confirmed the suitability of the TN LC device for use in polarimetry. A comparison of the results obtained with the TN LC device with the wave plates are presented in Table 3.5. The results achieved by the TN LC device are different for minimal tomography and HVDARL tomography. HVDARL mode of the device brings better results that are close to the wave plate analysis. The main difference between the device in HVDARL mode and wave plates in polarization analysis lies in the inaccuracy of reconstruction of the left-hand circular polarization. The cause of this imperfection will be further studied.

Another important advantage of the TN LC device is its ability to significantly accelerate polarization analysis. The total analysis duration can be reduced by factor 5-8, depending on the used sequence of projection and the choice tomographic method. However, to achieve this acceleration, it is necessary to apply the TN LC device in experiments where the preparation or analysis of the polarization state takes longer time than others part. Otherwise, the positive benefits of faster polarization adjustment are lost while waiting for other experiment peripherals, such as counters, wave plates, communication and others.

As the time response analysis of the TN LC device shows, it is right to look for a suitable projector sequence that will be used for the tomography of the polarizing state. Sometimes it may not be advisable to decrease the number of projections in order to achieve the shortest time of tomography. However, the reduce the number of projectors does not always lead to the best state estimation. Simulations that are presented in this thesis demonstrate the positive influence of the increasing number of projections for the measurement of one input polarization state. Based on the simulations, we can say that the increasing number of projectors has a positive effect on the quality of the reconstructed states of polarization. By doing so, we have made the reduction of the MSE value achieved by the device from 9.3(6) for mutually unbiased bases to 5.4(2) for nearly covariant measurement that uses 60 projectors.

For these reasons, we will continue to work on the development of TN LC devices and their applications. Last but not least, we would like to perform experimental verification of simulation results presented in the chapter 4.

Bibliography

[1] J. M. Bueno, "Polarimetry using liquid-crystal variable retarders: theory and calibration," *Journal of Optics A: Pure and Applied Optics*, vol. 2, no. 3, pp. 216–222, 2000.

[2] A. D. Martino, Y.-K. Kim, E. Garcia-Caurel, B. Laude, and B. Drévillon, "Optimized mueller polarimeter with liquid crystals," *Optics Letters*, vol. 28, no. 8, pp. 616–618, 2003.

[3] I. Moreno, J. L. Martínez, and J. A. Davis, "Two-dimensional polarization rotator using a twisted-nematic liquid-crystal display," *Applied Optics*, vol. 46, no. 6, pp. 881–887, 2007.

[4] S. L. Blakeney, S. E. Day, and J. N. Stewart, "Determination of unknown input polarisation using a twisted nematic liquid crystal display with fixed components," *Optics Communications*, vol. 214, no. 1-6, pp. 1–8, 2002.

[5] A. Peinado, A. Lizana, J. Vidal, C. Iemmi, and J. Campos, "Optimization and performance criteria of a stokes polarimeter based on two variable retarders," *Optics Express*, vol. 18, no. 10, pp. 9815–9830, 2010.

[6] A. Peinado, A. Lizana, J. Vidal, C. Iemmi, and J. Campos, "Optimized stokes polarimeters based on a single twisted nematic liquid-crystal device for the minimization of noise propagation," *Applied Optics*, vol. 50, no. 28, pp. 5437–5445, 2011.

[7] Y. August and A. Stern, "Compressive sensing spectrometry based on liquid crystal devices," *Optics Letters*, vol. 38, no. 23, p. 4996, 2013.

[8] Z. Zhuang, S.-W. Suh, and J. S. Patel, "Polarization controller using nematic liquid crystals," *Optics Letters*, vol. 24, no. 10, pp. 694–696, 1999.

[9] B. Ma, B. Yao, Z. Li, and T. Ye, "Improvement of the performance of the twisted-nematic liquid-crystal display as a phase modulator," *Applied Optics*, vol. 50, no. 17, p. 2588, 2011.

[10] J. Nicolás, J. Campos, and M. J. Yzuel, "Phase and amplitude modulation of elliptic polarization states by nonabsorbing anisotropic elements: application to liquid-crystal devices," *Journal of the Optical Society of America A*, vol. 19, no. 5, p. 1013, 2002.

[11] H.-K. Liu, J. A. Davis, and R. A. Lilly, "Optical-data-processing properties of a liquid-crystal television spatial light modulator," *Optics Letters*, vol. 10, no. 12, p. 635, 1985.

[12] U. Efron, *Spatial Light Modulator Technology: Materials, Devices, and Applications*. Optical Science and Engineering, Taylor & Francis, 1994.

[13] C. Rosales-Guzmán, A. Forbes, and S. of Photo-optical Instrumentation Engineers, *How to Shape Light with Spatial Light Modulators*. SPIE. Spotlight, SPIE Press, 2017.

[14] N. A. Riza, "High-optical-isolation low-loss moderate-switching-speed nematic liquid-crystal optical switch," *Optics Letters*, vol. 19, no. 21, p. 1780, 1994.

[15] R. A. Soref and D. H. McMahon, "Calcite 2 × 2 optical bypass switch controlled by liquid-crystal cells," *Optics Letters*, vol. 7, no. 4, p. 186, 1982.

[16] O. Aharon and I. Abdulhalim, "Liquid crystal lyot tunable filter with extended free spectral range," *Optics Express*, vol. 17, no. 14, p. 11426, 2009.

[17] J. Řeháček, B.-G. Englert, and D. Kaszlikowski, "Minimal qubit tomography," *Physical Review A*, vol. 70, no. 5, 2004.

[18] A. Ling, K. P. Soh, A. Lamas-Linares, and C. Kurtsiefer, "Experimental polarization state tomography using optimal polarimeters," *Physical Review A*, vol. 74, no. 2, 2006.

[19] W. K. Wootters and B. D. Fields, "Optimal state-determination by mutually unbiased measurements," *Annals of Physics*, vol. 191, no. 2, pp. 363–381, 1989.

[20] H. Zhu, "Quantum state estimation with informationally overcomplete measurements," *Physical Review A*, vol. 90, no. 1, 2014.

[21] J. Řeháček, Y. S. Teo, and Z. Hradil, "Determining which quantum measurement performs better for state estimation," *Physical Review A*, vol. 92, no. 1, 2015.

[22] D. Koutný, Y. S. Teo, Z. Hradil, and J. Řeháček, "Fast universal performance certification of measurement schemes for quantum tomography," *Physical Review A*, vol. 94, no. 2, 2016.

[23] J. Beeckman, "Liquid-crystal photonic applications," *Optical Engineering*, vol. 50, no. 8, p. 081202, 2011.

[24] Saleh and M. Teich, *Fundamentals of Photonics*. Wiley Series in Pure and Applied Optics, Wiley, 2007.

[25] D. Andrienko, "Introduction to liquid crystals," *Journal of Molecular Liquids*, vol. 267, pp. 520–541, 2018.

[26] J. Hoogboom, T. Rasing, A. E. Rowan, and R. J. M. Nolte, "LCD alignment layers. controlling nematic domain properties," *J. Mater. Chem.*, vol. 16, no. 14, pp. 1305–1314, 2006.

[27] J. Hoogboom, J. A. Elemans, A. E. Rowan, T. H. Rasing, and R. J. Nolte, "The development of self-assembled liquid crystal display alignment layers," *Philosophical Transactions of the Royal Society A: Mathematical, Physical and Engineering Sciences*, vol. 365, no. 1855, pp. 1553–1576, 2007.

[28] K. Takatoh, M. Sakamoto, R. Hasegawa, M. Koden, N. Itoh, and M. Hasegawa, *Alignment Technology and Applications of Liquid Crystal Devices*. Liquid Crystals Book Series, Taylor & Francis, 2005.

[29] D. Pauluth and K. Tarumi, "Advanced liquid crystals for television," *Journal of Materials Chemistry*, vol. 14, no. 8, p. 1219, 2004.

[30] D.-K. Yang and S.-T. Wu, *Fundamentals of liquid crystal devices, 2nd Edition*. Wiley, 2014.

[31] S. H. Perlmutter, D. Doroski, and G. Moddel, "Degradation of liquid crystal device performance due to selective adsorption of ions," *Applied Physics Letters*, vol. 69, no. 9, pp. 1182–1184, 1996.

[32] T. Geelhaar, "Liquid crystals for display applications," *Liquid Crystals*, vol. 24, no. 1, pp. 91–98, 1998.

[33] A. Yariv and A. P. Yeh, *Optical waves in crystals propagation and control of laser radiation*. J. Wiley & sons, 2003.

[34] I. Moreno, N. Bennis, J. A. Davis, and C. Ferreira, "Twist angle determination in liquid crystal displays by location of local adiabatic points," *Optics Communications*, vol. 158, no. 1-6, pp. 231–238, 1998.

[35] J. A. Davis, I. Moreno, and P. Tsai, "Polarization eigenstates for twisted-nematic liquid-crystal displays," *Applied Optics*, vol. 37, no. 5, pp. 937–945, 1998.

[36] C. Iemmi, "Quantitative prediction of the modulation behavior of twisted nematic liquid crystal displays based on a simple physical model," *Optical Engineering*, vol. 40, no. 11, p. 2558, 2001.

[37] M. Yamauchi, "Jones-matrix models for twisted-nematic liquid-crystal devices," *Applied Optics*, vol. 44, no. 21, p. 4484, 2005.

[38] D. A. Yakovlev, V. G. Chigrinov, and H.-S. Kwok, eds., *Modeling and Optimization of LCD Optical Performance*. John Wiley & Sons, Inc., 2015.

[39] T. A. F. König, P. A. Ledin, J. Kerszulis, M. A. Mahmoud, M. A. El-Sayed, J. R. Reynolds, and V. V. Tsukruk, "Electrically tunable plasmonic behavior of nanocube–polymer nanomaterials induced by a redox-active electrochromic polymer," *ACS Nano*, vol. 8, no. 6, pp. 6182–6192, 2014.

[40] V. Tkachenko, G. Abbate, A. Marino, F. Vita, M. Giocondo, A. Mazzulla, F. Ciuchi, and L. D. Stefano, "Nematic liquid crystal optical dispersion in the visible-near infrared range," *Molecular Crystals and Liquid Crystals*, vol. 454, no. 1, pp. 263/[665]–271/[673], 2006.

[41] D. Vašinka, "Bachelor's thesis." In progress, expected 2020.

[42] M. Bielak, "Elektrooptická manipulace s fotonickými kvantovými bity," 2017.

[43] A. Peinado, A. Lizana, and J. Campos, "Use of ferroelectric liquid crystal panels to control state and degree of polarization in light beams," *Optics Letters*, vol. 39, no. 3, pp. 659–662, 2014.

[44] Z. Hradil, J. Řeháček, J. Fiurášek, and M. Ježek, "3 maximum-likelihood methodsin quantum mechanics," in *Quantum State Estimation*, pp. 59–112, Springer Berlin Heidelberg, 2004.

[45] D. M. Greenberger, M. A. Horne, and A. Zeilinger, "Going beyond bell's theorem," in *Bell's Theorem, Quantum Theory and Conceptions of the Universe*, pp. 69–72, Springer Netherlands, 1989.

[46] J.-W. Pan, D. Bouwmeester, M. Daniell, H. Weinfurter, and A. Zeilinger, "Experimental test of quantum nonlocality in three-photon greenberger–horne–zeilinger entanglement," *Nature*, vol. 403, no. 6769, pp. 515–519, 2000.

[47] Meadowlark Optics, Inc, "Response time in liquid-crystal variable retarders," 2005.

[48] G. M. D. Ariano, P. Perinotti, and M. F. Sacchi, "Informationally complete measurements and group representation," *Journal of Optics B: Quantum and Semiclassical Optics*, vol. 6, no. 6, pp. S487–S491, 2004.

[49] R. B. A. Adamson and A. M. Steinberg, "Improving quantum state estimation with mutually unbiased bases," *Physical Review Letters*, vol. 105, no. 3, 2010.

[50] A. I. Lvovsky and M. G. Raymer, "Continuous-variable optical quantum-state tomography," *Reviews of Modern Physics*, vol. 81, no. 1, pp. 299–332, 2009.

[51] A. Ling, A. Lamas-Linares, and C. Kurtsiefer, "Accuracy of minimal and optimal qubit tomography for finite-length experiments," 2008.

[52] Y. S. Teo, H. Zhu, and B.-G. Englert, "Product measurements and fully symmetric measurements in qubit-pair tomography: A numerical study," *Optics Communications*, vol. 283, no. 5, pp. 724–729, 2010.